ARTICLE

# Raman Spectra of 1,2,4-Triazole-3-carboxylate Solution

Xue-fei Chen, Wei Fan, Xiao-guo Zhou*, Shi-lin Liu

*Hefei National Laboratory for Physical Sciences at the Microscale, iChEM (Collaborative Innovation Center of Chemistry for Energy Materials), Department of Chemical Physics, University of Science and Technology of China, Hefei 230026, China*

(Dated: Received on March 22, 2019; Accepted on April 22, 2019)

Raman spectra of 1,2,4-triazole-3-carboxylate ($TC^-$ anion) and its ring-deprotonated derivative ($dpTC^{2-}$ dianion) in aqueous solutions were measured respectively. The density functional theory calculations were performed using MN15 functional and PCM solvent model to investigate their structures, as well as the vibrational frequencies and Raman intensities. With the aid of the calculated spectra, all the observed Raman bands of $dpTC^{2-}$ were clearly assigned, with taking into account the deuteration shifts. Moreover, various protonic tautomers of $TC^-$ anion were compared in the present theoretical calculations, and 2H-tautomer was found more stable. The experimental Raman spectrum of $TC^-$ solution was roughly consistent with the calculated spectrum of the monomeric 2H-tautomer of $TC^-$, but some splits existed for a few bands when compared to the calculated spectra, which might be contributed by the hydrogen-bonding dimers of $TC^-$.

**Key words:** 1,2,4-Triazole-3-carboxylate, Raman spectrum, Density functional theory, Deprotonation

## I. INTRODUCTION

Triazoles have attracted much attention because of their important applications in various areas [1–13]. In bio-medical engineering, the triazole-ring is always utilized as the fundamental structure of many clinical drugs, *e.g.*, ribavirin, fluconazole, anastrozole, estazolam, and so on. Moreover, the triazole derivatives are extensively used as the corrosion inhibitors for metal/alloy protection [7–10]. In recent years, the prosperity of click-chemistry also makes the triazole derivatives be active subjects in synthetic chemistry [11–13].

Surface-enhanced Raman scattering (SERS) of triazole derivatives has been intensively studied to reveal the anti-corrosion mechanism of these compounds [14–25]. Various structural and bonding information on surfaces, such as adsorption orientation [14, 22, 24], self-assembled monolayer formation [22], competitive adsorption [20], and the influence of electrode potentials [20–22, 24, 25], were investigated. Through comparing the Raman spectra of these compounds in solutions and the SERS spectra, the assignments of the observed SERS bands were obtained, and then the interactions between the adsorbents and substrates were discussed [14–18, 24, 25].

It is well-known that Raman spectra in solutions are useful in disclosing the solute-solute/solute-solvent intermolecular interaction and the influences of solvent on quantum state energies of solute [25–29]. Wrzosek *et al.* performed Raman spectroscopy and DFT calculations on 3-sulfur derivatives of 1,2,4-triazole (TS) in solid state and in aqueous solutions at different pH values [25]. It was found that the solid sample consisted of the 3,3′-disulfide of the triazole dimer, while the disulfide bridge was broken in solutions. Interestingly, in solutions at various pH values, TS can exist in different molecular structures, *e.g.*, thiolate anions, thiol-thione tautomers, and a mixture of neutral thiol-thione tautomers and TS-thiol ring cation [25]. Meng *et al.* utilized vibrational spectroscopy and DFT calculation to study the environment-dependent conformation of 3-amino-1,2,4-triazole [26]. The dimers dominated in solid, but the monomers were the major component in polar solvents. The observed differences in vibrational frequency and intensity of Raman bands were mainly attributed to the perturbation of the intermolecular hydrogen bonding between amino-triazole and the protonic solvents.

Carboxylic substitution is a common strategy to modulate the electronic properties of organic compounds. Carboxylic substituted triazoles have been applied in biomedicine [3–6] and corrosion inhibition [10]. The plentiful nitrogen and oxygen atoms in triazole carboxylates provide versatile ways to combine metal atoms, making them be the useful ligands for constructing the coordinate co-polymers or the metal organic framework materials with novel structures [29–35]. Yurdakul and Tanribuyurdu performed the DFT calculations of the molecular geometry, relative energy,

*Author to whom correspondence should be addressed. E-mail: xzhou@ustc.edu.cn

 

and vibrational properties of several tautomers of 1,2,4-triazole-3-carboxylic acid (TCA), and the conclusions agreed with the FT-IR and Raman spectra of TCA measured in solid form [36]. As far as we know, the Raman spectra of triazole carboxylates in solutions have not been investigated yet, although their structures and properties in solutions are of great significance to understand the action mechanisms of the relative drugs and to optimize the hydrothermal syntheses conditions of the relative organometallic or coordination materials. Herein, we have measured the Raman spectra of 1,2,4-triazole-3-carboxylate and its deuterated derivatives in neutral and alkaline conditions. With the aid of the DFT calculations, the vibrational bands have been assigned, and their contributors have been discussed. All the conclusions can provide the detailed information of intermolecular hydrogen bonding.

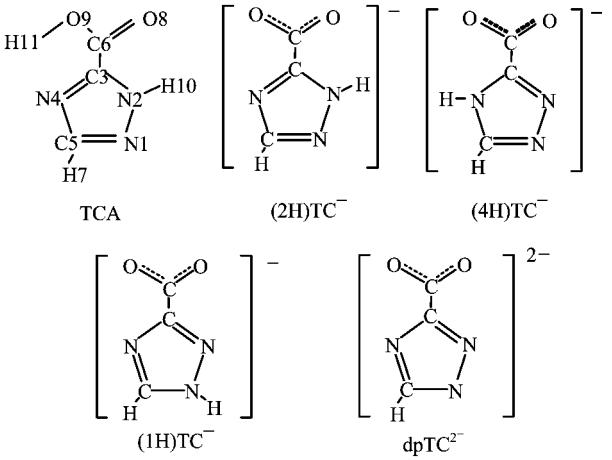


FIG. 1 Structural sketch with atomic labels for 1,2,4-triazole-3-carboxylic acid (TCA), three tautomers of 1,2,4-triazole-3-carboxylate anion ($TC^-$), and the deprotonated 1,2,4-triazole-3-carboxylate dianion ($dpTC^{2-}$).

## II. EXPERIMENTS

TCA (>97%) was purchased from Sigma-Aldrich and was used without further purification. Similar to other aromatic organic acids, the solubility of TCA in water was quite small (about 0.007 mol/L at room temperature). Thus, TCA was dissolved in two different NaOH aqueous solutions in the present experiments. In the first solution, 56.4 mg (0.0005 mol) TCA was completely dissolved into 1.0 mL of 0.5 mol/L NaOH aqueous solutions. The final pH value was about 7.0, indicating the occurrence of acid-alkaline neutralization. Thus, TCA was expected to exist as triazole carboxylate (noted as $TC^-$ hereafter). In the second solution, 56.5 mg TCA was completely dissolved in 1.0 mL of 1.2 mol/L NaOH aqueous solutions. The final pH was about 13.0, indicating a strong alkaline environment. Thus, TCA should undergo the deprotonation for the triazole ring (T-ring), and the major component became the deprotonated species and was marked as $dpTC^{2-}$ dianion for convenience. In both solutions, the concentration of TCA was the same as 0.5 mol/L. Similarly, two deuterated solutions were prepared by using heavy water ($D_2O$, 99.5%) and NaOD (95%). To promote the isotope substitution, the solution was sealed in a small bottle, and was water-bath incubated at 75 °C for 12 h. As the results, for $TC^-$ in the first solution, the H10 atom on the N atom and the H7 atom attached on C5 atom were replaced by deuterium, and hence the isotope substituted sample was denoted as d-$TC^-$. The deuterated $dpTC^{2-}$ (marked as d-$dpTC^{2-}$) was prepared by adding excessive NaOD to remove deuterium on the N atom of T-ring. The structures of TCA, three main tautomers of $TC^-$, and $dpTC^{2-}$, are shown in FIG. 1.

Raman spectra were recorded with a LABRAM-010 Raman spectrometer equipped with an air-cooled CCD detector, where a 600 groove/mm grating was used. The emission line at 488.0 nm of an $Ar^+$ ion laser was utilized as the excitation source with the power 3.5 mW on the samples. The acquisition time of the CCD detector was typically 100 s for Raman measurements. The spectra were baseline-subtracted.

All the DFT calculations were carried out using Truhlar's hybrid meta-NGA exchange-correlation functional MN15 [37]. The standard 6-311++G(d,p) basis sets and the PCM solvent model were employed in the present calculations. The optimized structures of TCA and its derivatives were obtained without symmetry constraint. Based on the optimized geometries, the analytic frequency calculations were performed to confirm their features of the global energy minimums, and to calculate the harmonic vibrational frequencies and the corresponding Raman activities. As the frequency scaling factor of the PCM-MN15/6-311++G(d,p) method was not found in literature, we conducted an auxiliary optimization-frequency calculation for benzene at the same level of theory. The calculated frequencies were then compared to the well-known 20 experimental frequencies of benzene in the region of <1700 $cm^{-1}$ [38], which gave a frequency scaling factor of 0.9818. This value was used in the present study. All the DFT calculations were performed with the Gaussian 16 program [39].

The relative Raman intensity was converted from the calculated Raman activity using the following formula derived from the basic theory of Raman scattering [40, 41]:

$$I_i = \frac{f(\nu_0 - \nu_i)^4 A_i}{\nu_i \left[1 - \exp(-hc\nu_i / k_{\mathrm{B}} T)\right]} \tag{1}$$

where $\nu_0$ is the frequency of excitation light, $\nu_i$ and $A_i$ are the harmonic frequency and Raman activity of the normal mode, $h$, $c$, and $k_{\mathrm{B}}$ are the well-defined fundamental constants, and $f$ is a suitably chosen intensity normalization factor independent of normal modes.

DOI:10.1063/1674-0068/cjcp1903060 

Based on the calculated Raman intensities and harmonic frequencies, the Raman spectra were simulated with Lorentzian line-shapes with a FWHM of 6 $cm^{-1}$. Assignments of vibrational frequencies were carried out by inspecting the atomic displacements of the corresponding normal modes in conjunction with the potential energy distribution (PED) analyses. The PED calculations were done with Jamróz's VETA 4.0 program [42, 43].

## III. RESULTS AND DISCUSSION

### A. Raman spectra of TCA in solutions at different alkalinity

The spectral contributors of TCA in solutions at different pH values can be changed from $TC^-$ in a neutral aqueous solution to $dpTC^{2-}$ dianion in strong alkaline environment. Thus, the changes of Raman spectra of TCA in $NaOH/H_2O$ solution were specially paid attention to with the increase of alkalinity. In the prepared neutral solution, the initial concentrations were 0.5 mol/L for both TCA and NaOH. By gradually adding 0.024 mL of 2.5 mol/L NaOH aqueous solution into the 1 mL solution of TCA, Raman spectra were measured as shown in FIG. 2(a). With the increase of NaOH concentration, the 1063, 1263, 1353, and 1453 $cm^{-1}$ bands were gradually enhanced, while the 983, 1108, 1279, 1341, and 1424 $cm^{-1}$ band intensities reduced, which responded to the transformation from the $TC^-$ anion to the ring-deprotonated $dpTC^{2-}$ dianion. Thus, these Raman bands must be contributed by $dpTC^{2-}$ dianion and $TC^-$ anion. Two strong bands at 1453 and 1263 $cm^{-1}$ in strong alkaline environment were not observed in neutral solution, and thus they could be used as the characteristic bands for $dpTC^{2-}$ dianion. Similarly, the band at 1424 $cm^{-1}$ in neutral solutions could be considered as the spectral marker for $TC^-$ anion, as it almost completely disappeared in strong alkaline solutions.

Since the 1453 $cm^{-1}$ band of $dpTC^{2-}$ and the 1424 $cm^{-1}$ band of $TC^-$ are well separated from the other bands, their intensity changes can reflect the transformation from $TC^-$ to $dpTC^{2-}$ with the increase of alkalinity. FIG. 2(b) plots the intensity changes of the bands at 1453 and 1424 $cm^{-1}$ *vs.* the molar concentration ratio of [NaOH]/[TCA]. From the unchanged stages in FIG. 2(b), the complete transformation from the $TC^-$ anion to the $dpTC^{2-}$ dianion can be estimated to occur at the [NaOH]/[TCA] ratio of ∼2.05. Moreover, as shown in assignment of the vibrational bands in the following sections, all the bands in FIG. 2(a) can be attributed to $dpTC^{2-}$ and $TC^-$, implying that TCA exists only as the conformations of $dpTC^{2-}$ or $TC^-$ in aqueous solution.

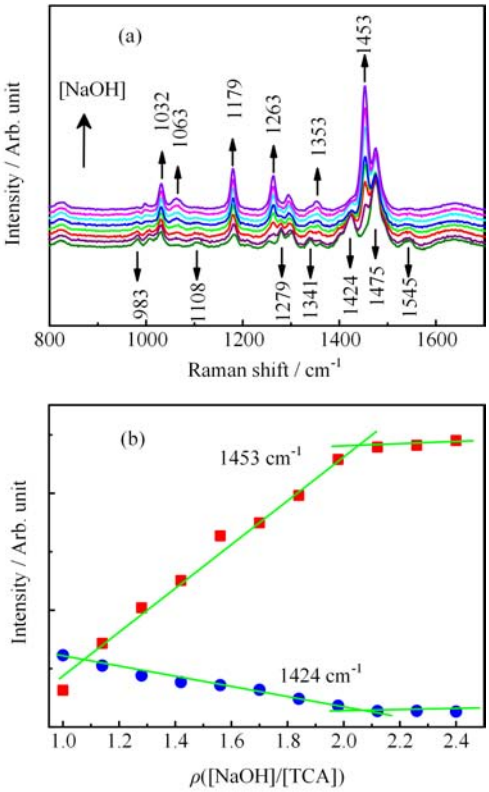


FIG. 2 (a) Raman spectra with step-by-step adding 0.024 mL NaOH solution (2.5 mol/L) into 1 mL the alkaline solution of TCA. The initial concentration of TCA is 0.5 mol/L in alkaline solutions. (b) Intensities of the two bands at 1453 and 1424 $cm^{-1}$ *vs.* the molar concentration ratio of [NaOH]/[TCA].

### B. Assignments of the Raman bands for $dpTC^{2-}$ dianion

FIG. 3 shows the experimental and calculated Raman spectra of $dpTC^{2-}$ dianion and its H7-deuterated derivative d-$dpTC^{2-}$ in solutions. Both the concentration ratios, [NaOH]/[TCA] and [NaOD]/[TCA], were 2.4 for the solutions of TCA in $NaOH/H_2O$ and $NaOD/D_2O$ solutions. As shown in FIG. 3 (a) and (b), the spectrum of $NaOD/D_2O$ solution is almost identical to that of $NaOH/H_2O$, whatever for the peak positions and intensity patterns. The only difference exists at 1580 $cm^{-1}$ where a weak band is observed in the $NaOD/D_2O$ solution, and its counterpart may be masked by the broad $H_2O$ bending band (centered at ∼1640 $cm^{-1}$) in the $NaOH/H_2O$ solution. The lack of isotopic effect provides an unambiguous evidence that in strong alkaline environment, $TC^-$ undergoes deprotonation for the labile hydrogen atom (H10) on the N-atom of T-ring. FIG. 3(c) shows the recorded Raman spectrum of H7-deuterated sample, d-$dpTC^{2-}$, in alkaline $NaOD/D_2O$ solution ([NaOD]/[TCA]=2.4). Compared with FIG. 3(c), the evident differences can be observed in FIG. 3(a).

DOI:10.1063/1674-0068/cjcp1903060 

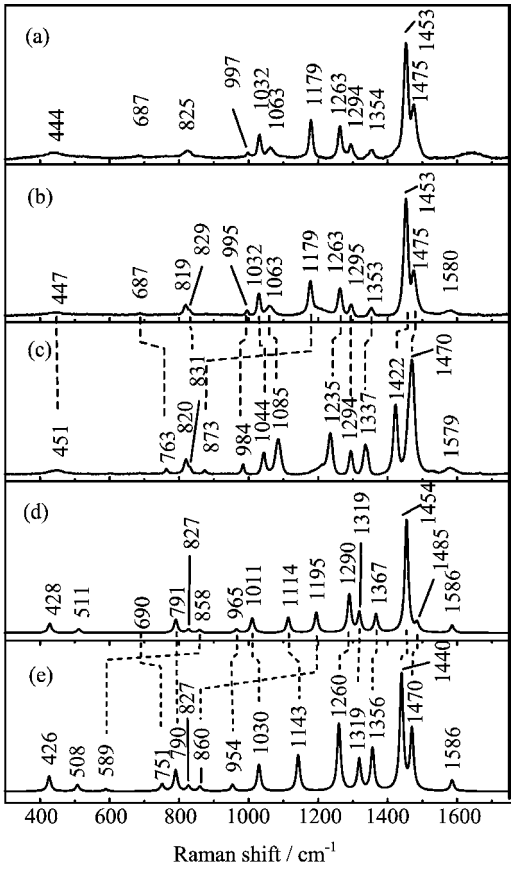


FIG. 3 Experimental (a, b, c) and calculated (d, e) Raman spectra of $dpTC^{2-}$ and d-$dpTC^{2-}$. (a) $dpTC^{2-}$ in $NaOH/H_2O$ solution, (b) $dpTC^{2-}$ in $NaOD/D_2O$ solution, (c) d-$dpTC^{2-}$ in $NaOD/D_2O$ solution, (d) $dpTC^{2-}$ in $H_2O$, and (e) d-$dpTC^{2-}$ in $D_2O$.

Based on the optimized geometries of $dpTC^{2-}$ and d-$dpTC^{2-}$ dianions at the PCM-MN15/6-311++G(d,p) level, their Raman spectra are simulated and displayed in FIG. 3 (d) and (e), respectively. The structure parameters, including bond lengths, bond angles, and dihedral angles of $dpTC^{2-}$ dianion and $(2H)TC^-$ (the most stable tautomer of $TC^-$ anion) are listed in Table S1 of the supplementary materials. To our surprise, the simulated spectrum of $dpTC^{2-}$ in FIG. 3(d) agrees very well with the experimental Raman spectrum in FIG. 3(a), except for a little weak intensity of the 1475 $cm^{-1}$ band. For d-$dpTC^{2-}$, the agreement between the experimental and calculated spectra is also obtained as shown in FIG. 3 (c) and (e). Table I summarizes the spectral assignments of the major Raman bands for $dpTC^{2-}$ and d-$dpTC^{2-}$. The PEDs of $dpTC^{2-}$ are also provided in Table I.

According to the calculated PEDs, the Raman bands in the region of 1050−1650 $cm^{-1}$ are contributed by the T-ring in-plane bond stretching, CO stretching of the $COO^-$ group, and in-plane C5H7 bending modes. The C6O8/C6O9 anti-phase stretching of the $COO^-$ group contributes the weak band at 1586 $cm^{-1}$ for $dpTC^{2-}$ or d-$dpTC^{2-}$ in FIG. 3 (d) and (e), which agrees well with the experimental data of 1580 $cm^{-1}$ for $dpTC^{2-}$ and 1579 $cm^{-1}$ for d-$dpTC^{2-}$. The strong 1475 $cm^{-1}$ band of $dpTC^{2-}$ and its counterpart in d-$dpTC^{2-}$ (at 1470 $cm^{-1}$) are attributed to the T-ring N1C5/C5N4 anti-phase stretching vibration, whose frequencies are calculated as 1485 $cm^{-1}$ and 1470 $cm^{-1}$ for $dpTC^{2-}$ and d-$dpTC^{2-}$, respectively. Although the Raman intensity of this band is underestimated in calculations, the PCM-MN15 level of theory does correctly predict an impressive intensity increase of this band upon H7-deuteration. Moreover, the strong band at 1453 $cm^{-1}$ for $dpTC^{2-}$ and that at 1422 $cm^{-1}$ for d-$dpTC^{2-}$ in the experimental spectra are attributed to the N2C3/C3C6 anti-phase stretching strongly coupled with the N2C3N4 bending as well as the C6O8 stretching. This vibration was calculated at 1454 $cm^{-1}$ for $dpTC^{2-}$ and 1440 $cm^{-1}$ for d-$dpTC^{2-}$, respectively, and both of them were the strongest in the simulated Raman spectra of FIG. 3 (d) and (e). The 1353, 1295, and 1263 $cm^{-1}$ bands of $dpTC^{2-}$ in FIG. 3(b) are assigned to the N2C3/N1C5 anti-phase stretching, C3N4/N4C5 anti-phase stretching, and N4C5/C5N1 in-phase stretching, respectively. The former two also strongly coupled with O8C6/C6O9 in-phase stretching of $COO^-$ group. The calculated frequencies of them are 1367, 1319, and 1290 $cm^{-1}$, and the Raman intensities also closely resemble the experimental results. As shown in FIG. 3 and Table I, the calculated H7-deuteration shifts of these three modes are 11, 0, and 30 $cm^{-1}$, respectively, also well consistent with the observed values (16, 1, and 28 $cm^{-1}$) in experiments.

The C5H7 in-plane bending of $dpTC^{2-}$ is calculated to appear at 1195 $cm^{-1}$, which is contributed by the stretching vibrations of N1N2, N1C5, and N4C5 bonds (Table I). Experimentally, a strong band at 1179 $cm^{-1}$ was observed for $dpTC^{2-}$, but no band was detected nearby for d-$dpTC^{2-}$. This experimental peak is assigned to the C5H7 in-plane bending mode of $dpTC^{2-}$. The C5H7 in-plane bending mode is expected to show dramatic red-shift upon H7-deuteration, and according to PCM-MN15 calculation it shifts to 860 $cm^{-1}$. The weak band at 873 $cm^{-1}$ of d-$dpTC^{2-}$ in FIG. 3(c) may be contributed by this mode. The measured down-shift of 306 $cm^{-1}$ upon H7-deuteration is well consistent with the DFT prediction (335 $cm^{-1}$). Meanwhile, both theoretical and experimental results show an intensity decrease for this mode upon H7-deuteration.

The band at 1063 $cm^{-1}$ of $dpTC^{2-}$ in FIG. 3(b) is assigned to N1N2 stretching, which is calculated at 1114 $cm^{-1}$ in FIG. 3(d). The H7-deuteration causes an unusual upward shift for this mode by 22 $cm^{-1}$ and 29 $cm^{-1}$, respectively, according to the experiment and the calculation. In addition, both the experiments and the calculations manifest an increase in Raman intensity upon H7-deuteration. By inspecting the atomic displacements of corresponding modes, we found that the

DOI:10.1063/1674-0068/cjcp1903060 

TABLE I Experimental and calculated Raman frequencies (in $cm^{-1}$) of $dpTC^{2-}$ and d-$dpTC^{2-}$ dianions, as well as the potential energy distributions (PEDs) of $dpTC^{2-}$.

| Experimental frequency[a] | | Calculated frequency[b] | | Assignment[c] of $dpTC^{2-}$(PED/%) |
|---|---|---|---|---|
| $dpTC^{2-}$ | d-$dpTC^{2-}$ | $dpTC^{2-}$ | d-$dpTC^{2-}$ | |
| | | 3169 | 2349 | $\nu$C5H7(+99) |
| 1580(m) | 1579(m) | 1586 | 1586 | $\nu$C6O8(−46), $\nu$C6O9(+46) |
| 1475(s) | 1470(vs) | 1485 | 1470 | $\nu$N1C5(+21), $\nu$N4C5(−17), $\nu$N4C3(−20), $\delta$N1C5H7(−19) |
| 1453(vs) | 1422(vs) | 1454 | 1440 | $\nu$N2C3(−27), $\nu$C3C6(+22), $\nu$C6O8(−13), $\delta$N2C3N4(+13) |
| 1353(m) | 1337(s) | 1367 | 1356 | $\nu$N2C3(+46), $\nu$N1C5(−16), $\nu$C6O9(−14) |
| 1295(m) | 1294(s) | 1319 | 1319 | $\nu$N4C3(+44), $\nu$C6O8(−18), $\nu$C6O9(−12), N4C5(−10) |
| 1263(s) | 1235(s) | 1290 | 1260 | $\nu$N4C5(+47), $\nu$N1C5(+42) |
| 1179(s) | 873(w) | 1195 | 860 | $\delta$H7C5N1(+45), $\nu$N1N2(−18), $\nu$N4C5(−16), $\nu$N1C5(+11) |
| 1063(m) | 1085(s) | 1114 | 1143 | $\nu$N1N2(+73), $\delta$N1C5H7(+15) |
| 1032(s) | 1044(s) | 1011 | 1030 | $\delta$N4C3N2(+39), $\nu$N4C3(+24), $\nu$N2C3(+12) |
| 995(w) | 984(m) | 965 | 954 | $\delta$C5N1N2(+87) |
| | | 858 | 589 | $\tau$H7C5N1N2(+84), $\tau$C3C5N2N1(−11) |
| 829(sh) | 831(sh) | 827 | 827 | $\tau$C6O9O8C3(−64), $\tau$C3C6N2N4(+20), $\tau$C3N2N4C5(+14) |
| 819(m) | 820(m) | 791 | 790 | $\delta$O9C6O8(+64), $\delta$N4C3N2(−14) |
| 687(vw) | 763(w) | 690 | 751 | $\tau$C3C5N2N1(+84), $\tau$H7C4N1N2(+13) |
| | | 676 | 681 | $\tau$C3N2N4C5(+69), $\tau$C6O9O8C3(−24) |
| | | 511 | 508 | $\delta$O8C6C3(+59), $\tau$C6C3N2(−24) |
| 447(w) | 451(w) | 428 | 426 | $\nu$C6C3(+51), $\delta$O9C6O8(−27), $\delta$N4C3N2(−17) |
| | | 243 | 240 | $\delta$C6C3N2(+61), $\delta$O8C6C3(+28) |
| | | 207 | 201 | $\tau$C3C6N2N4(+73) |
| | | 69 | 68 | $\tau$O8C6C3N4(+99) |

[a] vs: very strong, s: strong, m: medium, w: weak, vw: very weak, sh: shoulder peak. Solvent: $D_2O$.
[b] Frequency scaling factor of 0.9818 was used.
[c] $\nu$: bond stretching, $\delta$: in-plane bending, $\tau$: out-of-plane torsion, +/− in parentheses: in-phase/anti-phase changes of the internal coordinates. .

N1N2 stretching is severely coupled with the C5−H7 in-plane bending for $dpTC^{2-}$, whereas this type of coupling is very weak for d-$dpTC^{2-}$. Thus, the blue isotopic shift of this mode and the increase of Raman intensity are attributable to the considerable change of the normal mode composition after H7-deuteration.

The Raman bands in the region less than 1050 $cm^{-1}$ involve in-plane and out-of-plane deformations of T-ring, OCO bending of the $COO^-$ group, and relative motions between T-ring and $COO^-$ group. The 1032 $cm^{-1}$ band of $dpTC^{2-}$ in FIG. 3(b) is assigned to the T-ring in-plane deformation involving mainly N4C3N2 bending, corresponding to the 1011 $cm^{-1}$ band in the calculated spectrum of FIG. 3(d). The H7-deuteration causes a blue shift for this mode by 12 $cm^{-1}$, which is comparable with the calculated value 19 $cm^{-1}$. The atomic displacements of this mode show that the C5−H7 in-plane bending is coupled with the T-ring deformation, but the phase is opposite for $dpTC^{2-}$ and d-$dpTC^{2-}$. This may be responsible for the blue-shift of this mode by H7-deuteration. The band of $dpTC^{2-}$ at 995 $cm^{-1}$ in FIG. 3(b) is also a T-ring in-plane deformation mode, which involves mainly the C5N1N2 bending. This mode is calculated to appear at 965 $cm^{-1}$ and shows 11 $cm^{-1}$ red-shift upon H7-deuteration, well consistent with the experiments.

The Raman band at 819 $cm^{-1}$ in FIG. 3(b) is due to the O9C6O8 bending of $COO^-$ group, which is calculated at 791 $cm^{-1}$. The weak shoulder band at 829 $cm^{-1}$ in FIG. 3(b) is attributed to an out-of-plane vibration of T-ring, involving mainly the out-of-plane motion of C3 atom. The low-frequency band at 447 $cm^{-1}$ in FIG. 3(b) is attributed to the translation of the $COO^-$ group relative to the T-ring, along the direction of C3−C6 bond. The C3−C6 bond stretching contributes a large PED (51%) to this mode.

### C. Raman spectra of $TC^-$ anion

$TC^-$ has three main protonic tautomers, denoted here as (2H)$TC^-$, (1H)$TC^-$, and (4H)$TC^-$, respectively, in which the labile hydrogen atom is attached on N2, N1, and N4 atoms. In principle, $TC^-$ might have another four tautomers (see FIG. S1 in supplementary materials), in which the hydrogen atom is attached on

DOI:10.1063/1674-0068/cjcp1903060 

TABLE II Calculated energies ($E$ in atomic unit), Gibbs free energies ($G$ in atomic unit), relative energies ($\Delta E$ in kcal/mol), relative Gibbs free energies ($\Delta G$ in kcal/mol) of $dpTC^{2-}$, $TC^-$ tautomers, and dimeric $TC^-$.

| | | $E$ | $G$ | $\Delta E^a$ | $\Delta G^a$ |
|---|---|---|---|---|---|
| $dpTC^{2-}$ | | −429.56379 | −429.54513 | | |
| Tautomers | (2H)$TC^-$ | −430.04700 | −430.01512 | 0.00 | 0.00 |
| $TC^-$ | (4H)$TC^-$ | −430.04247 | −430.01138 | 2.84 | 2.35 |
| | (1H)$TC^-$ | −430.04142 | −430.01028 | 3.51 | 3.04 |
| Dimeric | Dimer 1 | −860.11421 | −860.03133 | 0.00 | 0.00 |
| $TC^-$ | Dimer 2 | −860.10889 | −860.02735 | 3.34 | 2.50 |
| | Dimer 3 | −860.10609 | −860.02412 | 5.10 | 4.53 |
| | Dimer 4 | −860.10466 | −860.02353 | 5.99 | 4.89 |
| | Dimer 5 | −860.10546 | −860.02355 | 5.49 | 4.88 |
| | Dimer 6 | −860.10428 | −860.02273 | 6.23 | 5.39 |

[a] Relative to (2H)$TC^-$ for $TC^-$ tautomers or relative to the dimer 1 for dimeric $TC^-$.

the O8 or O9 atoms. But in view that the p$K_a$ values of carboxylic acids are larger than those of azoles, these four carboxylic-acid type tautomers are unlikely to co-exist with (2H)$TC^-$/(1H)$TC^-$/(4H)$TC^-$ in solution. The PCM-DFT calculations also confirm that free energies of the four carboxylic-acid type tautomers are higher than (2H)$TC^-$ by at least 4.96 kcal/mol. Thus, the four carboxylic-acid type tautomers will not be discussed in the following sections. The optimized geometry parameters of (2H)$TC^-$, (1H)$TC^-$, and (4H)$TC^-$ are summarized in Table S2 of the supplementary materials. Using the optimized geometries, their relative energies and Gibbs free-energies are calculated and listed in Table II. Based on the relative free energies, the Boltzmann distributions of the three tautomers are determined to be 97.6% for (2H)$TC^-$, 1.8% for (4H)$TC^-$, and 0.6% for (1H)$TC^-$, indicating that the overwhelming majority of $TC^-$ anions exists as (2H)$TC^-$ at room temperature.

The simulated Raman spectra of (1H)$TC^-$, (4H)$TC^-$, and (2H)$TC^-$ are displayed in FIG. 4 (a), (b), and (c), repectively. FIG. 4(d) shows the experimental Raman spectrum of $TC^-$ in aqueous solution. Among the three tautomers, the calculated spectrum of (2H)$TC^-$ agrees better with the experimental spectrum. The slight differences seem not to be caused by the contributions of different tautomers, as the thermal distribution-weighted average spectrum in FIG. 4(e) is nearly identical to that of (2H)$TC^-$ alone in FIG. 4(c).

FIG. 5 shows the experimental spectra of $TC^-$ in aqueous solution and its deuterated derivative d-$TC^-$ in $D_2O$, together with the calculated spectra of (2H)$TC^-$ and d-(2H)$TC^-$. An initial impression can be obtained that some bands in experiments can be considered as split doublets of the single peaks in the calculated spectra. As discussed in the following section, the formation of dimer in solutions could contribute to the band splitting. In Table III, the correlation between the experimental frequencies of $TC^-$ and d-$TC^-$ and the calculated frequencies of (2H)$TC^-$ and d-(2H)$TC^-$ are listed, as well as the PED results of (2H)$TC^-$.

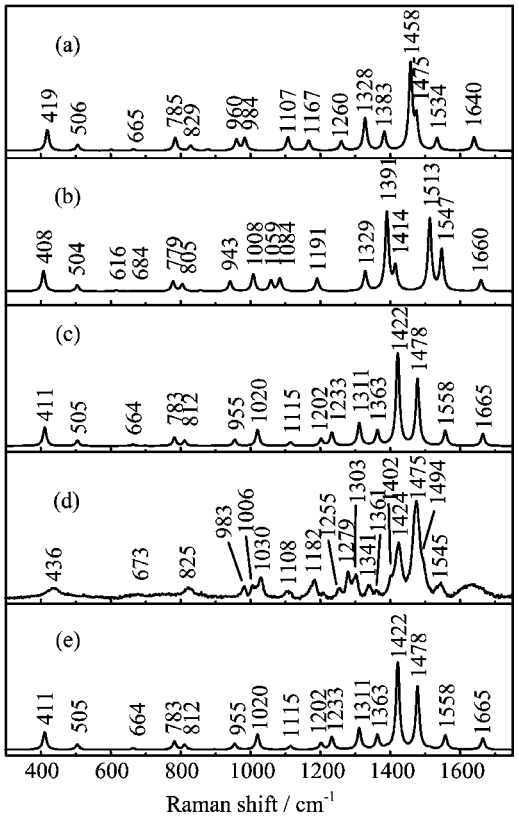


FIG. 4 The calculated Raman spectra of $TC^-$: (a) tautomer (1H)$TC^-$, (b) tautomer (4H)$TC^-$, (c) tautomer (2H)$TC^-$. (d) The experimental Raman spectrum of $TC^-$ in aqueous solution. (e) Tautomer-distribution-weighted avearge spectrum.

Based on Tables III, the assignments of the observed Raman peaks are obtained. The weak bands at 1619 $cm^{-1}$ observed in the $D_2O$ solution of d-$TC^-$ are attributed to the anti-phase O8C6/C6O9 stretch of $COO^-$ group. Compared to that of $dpTC^{2-}$, this mode shows a quite large blue-shift (by 39 $cm^{-1}$), owing to the interaction between the O8 and H10(D10) atoms. In FIG. 5(a), the weak and broad peak at 1545 $cm^{-1}$ of $TC^-$ corresponds to the calculated band at 1558 $cm^{-1}$ which is mainly contributed by the stretching of N4C3 and N1C5 bonds. The doublets at 1475/1494 (shoulder), 1424/1402 (shoulder), 1361/1341, and 1303/1279 $cm^{-1}$ correspond to the calculated peaks of (2H)$TC^-$ at 1478, 1422, 1363, and 1311 $cm^{-1}$ in FIG. 5(c). According to the calculated PEDs and atomic displacements, the bands at 1478 and 1422 $cm^{-1}$ in the calculated spectrum of FIG. 5(c)

DOI:10.1063/1674-0068/cjcp1903060 

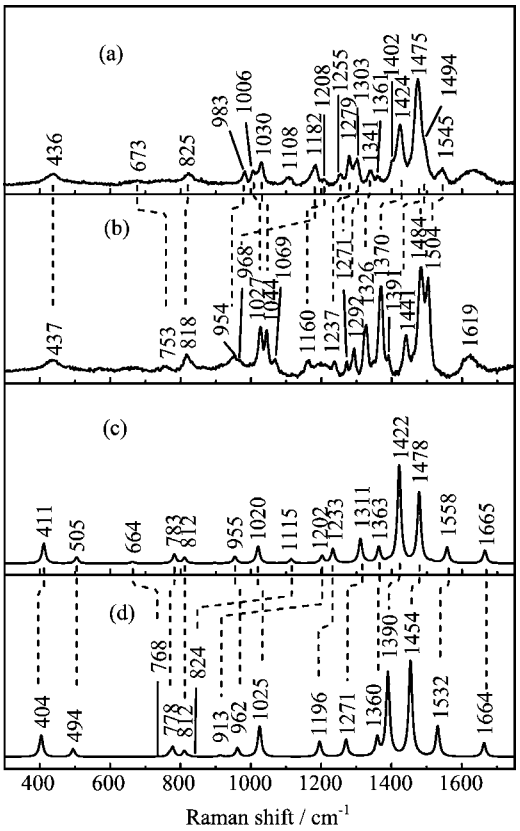


FIG. 5 The experimental Raman spectra of (a) $TC^-$ in $H_2O$ solution and (b) d-$TC^-$ in $D_2O$ solution; and the calculated Raman spectra of (c) (2H)$TC^-$ and (d) d-(2H)$TC^-$.

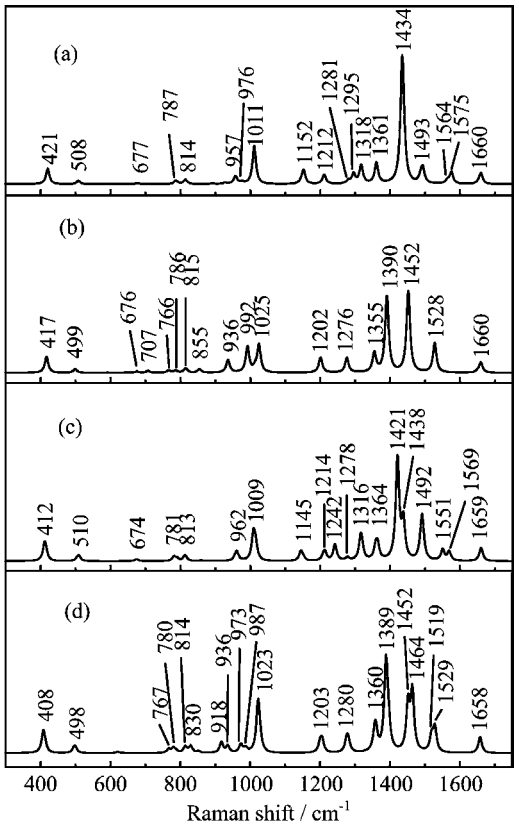


FIG. 6 The calculated Raman spectra of (a) dimer 1 and (b) dueterated dimer 1, (c) dimer 2 and (d) dueterated dimer 2.

are assigned to the T-ring in-plane skeleton vibrations involving the stretches of the N2C3 and N4C3/N1C5 bonds. The peak at 1363 $cm^{-1}$ is attributed to the in-phase O8C6/C6O9 stretch coupling with the N4C3 and N1C5 stretches, and that at 1311 $cm^{-1}$ comes from the N1C5/C5N4 anti-phase stretch.

The observed 1006/1030 $cm^{-1}$ doublet in FIG. 5(a) is considered to correlate to the calculated band at 1020 $cm^{-1}$ in FIG. 5(c), which is attributed to the T-ring in-plane deformation involving N2C3N4 bending and in-phase N4C3/N2C3 stretch. Like $dpTC^{2-}$, the in-plane deformation mode shows blue-shift upon deuteration. The band at 983 $cm^{-1}$ in FIG. 5(a) is also a T-ring in-plane deformation mode but involves mainly the C5N1N2 bending. The bands at 825, 673, and 436 $cm^{-1}$ in FIG. 5(a) are assigned, respectively, to the O8C6O9 bending, C3N2N4C5 out-of-plane torsion, and the translation of $COO^-$ group relative to the T-ring.

### D. DFT calculations on dimers of $TC^-$

As mentioned above, in comparison with the calculated spectra of (2H)$TC^-$ and d-(2H)$TC^-$, some double splits were observed in the experimental spectra of $TC^-$ and its deuterated derivatives. In contrast, $dpTC^{2-}$ exhibits almost one-to-one correspondence between the calculated and experimental bands. Thus, a reasonable presumption is drawn that the hydrogen-bonding interaction of the labile H10 atom on T-ring with neighboring molecules can cause the unusual double splits for $TC^-$. Using Raman/IR spectroscopy and DFT calculations, Meng *et al.* confirmed that 3-amino-1,2,4-triazole exists as monomers in solution but as dimers with hydrogen-bonding in solid state [26]. Taking into account that $TC^-$ contains three nitrogen and two oxygen atoms, the dimer formed by hydrogen-bonding could not be ruled out. The dimerization, if presents, would surely have strong effect on the Raman spectra. Especially, for a homodimer the local vibrational modes of the two molecules can couple with each other [44]. This so-called vibrational exciton coupling can cause double split of IR or Raman bands.

To verify this assumption, the structures of probable hydrogen-bonding dimers of $TC^-$ were optimized and are shown in FIG. S2 of the supplementary materials. Then the electronic energies and Gibbs free energies of them were calculated and are listed in Table II too. The two most stable dimers (dimers 1 and 2) are homodimers composed of two (2H)$TC^-$ anions.

DOI:10.1063/1674-0068/cjcp1903060 

TABLE III Correlation of the experimental Raman frequencies (in $cm^{-1}$ ) of $TC^-$ and d-$TC^-$ anions and the calculated ones of (2H)$TC^-$ and d-(2H)$TC^-$, together with the PED results of (2H)$TC^-$.

| Experimental frequency[a] | | Calculated frequency[b] | | Assignment of (2H)$TC^{2-}$(PED/%) |
|---|---|---|---|---|
| $TC^-$ in $H_2O$ | d-$TC^-$ in $D_2O$ | (2H)$TC^-$ | d-(2H)$TC^-$ | |
| | | 3593 | 2643 | $\nu$N2H10(+100) |
| | | 3224 | 2393 | $\nu$C5H7(+99) |
| | 1619(br) | 1665 | 1664 | $\nu$O9C6(−55), $\nu$O8C6(+40) |
| 1545(m)[c] | 1504(s) | 1558 | 1532 | $\nu$N4C3(+34), $\nu$N1C5(−15), $\nu$C3C6(−10), $\delta$H10N2N1(+12), $\delta$H7C5N4(−10), $\delta$N2C3N4(−10) |
| 1494(sh), 1475 (vs) | 1484(vs), 1441(s) | 1478 | 1454 | $\nu$N2C3(+42), $\nu$N1C5(+13), $\delta$H7C5N4(+11) |
| 1424(s), 1402(sh) | 1391(sh), 1370(vs) | 1422 | 1390 | $\nu$N4C3(−22), $\nu$N1C5(−15), $\delta$H10N2N1(+14) |
| 1361(w), 1341 (m) | 1326(s) | 1363 | 1360 | $\nu$O8C6(-33), $\nu$O9C6(-20), $\nu$N1C5(+16), $\nu$N4C3(+17) |
| 1303(m), 1279(m) | 1292(m), 1271(w) | 1311 | 1271 | $\nu$N4C5(+35), $\nu$N1C5(+28), $\nu$N1N2(−10) |
| 1255(m) | 1237(w) | 1233 | 1196 | $\nu$N1N2(−28), $\delta$H10N2N1(+24), $\nu$N2C3(−14) |
| 1208(w) | 1160(w) | | | |
| 1182(m,br) | 968(w,sh) | 1202 | 913 | $\delta$H7C5N4(+42), $\nu$N4C5(+37) |
| | 1069(w) | | | |
| 1108(w) | | 1115 | 824 | $\nu$N1N2(+39), $\delta$H10N2N1(+32) |
| 1030(m), 1006(m) | 1044(s), 1027(s) | 1020 | 1025 | $\delta$N2C3N4(+42), $\nu$N4C3(+17), $\nu$N2C3(+16) |
| 983(m) | 954(m,br) | 955 | 962 | $\delta$C5N1N2(+78) |
| | | 897 | 589 | $\tau$H7C5N4C3(+84), $\tau$C3N2N4C5(+12) |
| | | 812 | 812 | $\tau$C6O9O8C3(+64), $\tau$C3C6N4N2(+19), $\tau$C3N2N4C5(−12) |
| 825(br) | 818(br) | 783 | 778 | $\delta$O8C6O9(+65), $\delta$N2C3N4(−13) |
| | | 695 | 497 | $\tau$H10N2N1C5(+62), $\tau$C3C5N2N1(−29) |
| 673(w,br) | 753(vw) | 664 | 768 | $\tau$C3N2N4C5(+49), $\tau$H10N2N1C5(+22), $\tau$H7C5N4C3(−10), $\tau$C6O9O8C3(+10) |
| | | 627 | 634 | $\tau$C3C5N2N1(+54), $\tau$H10N2N1C5(+15), $\tau$C6O9O8C3(−14), $\tau$C3N2N4C5(−12) |
| | | 505 | 494 | $\delta$O8C6C3(+62), $\delta$C6C3N4(+21) |
| 436(w) | 437(w) | 411 | 404 | $\nu$C3C6(+50), $\tau$O8C6O9(−24), $\tau$N2C3N4(−17) |
| | | 201 | 193 | $\delta$C6C3N4(+66), $\delta$O8C6C3(−30) |
| | | 198 | 190 | $\tau$C3C6N4N2(+73), $\tau$C3N2N4C5(+12) |
| | | 76 | 60 | $\tau$O8C6C3N2(+94) |

[a] Raman spectra excited at 488 nm.
[b] scaling factor of frequency is 0.9818.

In dimer 1, two (2H)$TC^-$ anions are connected by two N−H···O hydrogen bonds, while in dimer 2 one N−H···O and one N−H···N hydrogen bonds connect two monomers. The other dimers (dimers 3−6) have the higher Gibbs free energies than dimer 2 by 2.0−2.9 kcal/mol, and thus they are less stable. The binding free energies, defined as the Gibbs free energy of the dimer minus the sum of that of two (2H)$TC^-$ monomers, are −0.68 kcal/mol for dimer 1 and 1.82 kcal/mol for dimer 2, respectively. Although the binding energy of dimer 2 is slightly positive, it may exist in solution in view of the high concentration of $TC^-$ in experiments.

FIG. 6 displays the simulated Raman spectra of dimers 1 and 2 as well as their deuterated derivatives. The vibrational frequencies and Raman activities are listed in Table S3 of the supplementary material. For most of vibrational modes of dimer 1, the excitonic splits induced by dimerization are small and typically vary less than 6 $cm^{-1}$. Only the N4C3/N1C5 anti-phase stretch and H10 in-plane bending modes, whose frequencies were 1558 and 1233 $cm^{-1}$ in (2H)$TC^-$ monomer, show evident splits in dimers 1 as 1575/1564 $cm^{-1}$ and 1295/1281 $cm^{-1}$, respectively. For dimer 2, only the N4C3/N1C5 anti-phase stretch and N4C3/N1C5 in-phase stretch show large splits into 1569/1551 $cm^{-1}$ and 1438/1421 $cm^{-1}$, respectively. Therefore, some other unknown factors, besides dimerization, should be responsible for the observed band splitting in experiments.

We noticed that, in addition to excitonic splits, many Raman bands of dimers 1 and 2 show considerable shifts in comparison to their counterparts in the monomeric

DOI:10.1063/1674-0068/cjcp1903060 

(2H)$TC^-$. Thus, the double splits in Raman spectra of $TC^-$ could be explained by co-existence of monomers and dimers (presumably as Dimer 1) in solutions. This deduction is acceptable, especially taking into account the small binding energy of dimer 1.

## IV. CONCLUSION

Raman spectra of $TC^-$ anion and $dpTC^{2-}$ dianion in $H_2O/D_2O$ solutions were measured and analyzed with the aid of the density functional theory at the MN15/6-311++G(d,p) level and PCM solvent model. Based on the optimized geometries, the frequencies and Raman activities of various vibrational modes were calculated. Then the Raman spectra of $TC^-$ anion and $dpTC^{2-}$ dianion were simulated to compare with the experimental data.

For $dpTC^{2-}$ and its deuterated derivative, the experimental Raman spectra were greatly consistent with the simulated spectra of the monomer. All dominant vibrational bands in spectra were well assigned.

Various protonic tautomers of $TC^-$ anion were checked with DFT calculations. The 2H-tautomer was found more stable than the others, and overwhelmingly dominated in solutions at room temperature. Interestingly, the experimental Raman spectrum of $TC^-$ anion was roughly consistent with the simulated spectrum of 2H-tautomer of $TC^-$, but double splits were observed for a few Raman bands. The stable hydrogen-bonding dimers of $TC^-$ were suggested to exist in solution, and the dimer-monomer equilibrium was inferred to be responsible for the splits.

**Supplementary materials:** DFT calculated structural parameters and structural sketches of the studied species are shown.

## V. ACKNOWLEDGEMENTS

This work was supported by the National Natural Science Foundation of China (No.21573208, No.21573210, and No.21873089) and the National Key Basic Research Foundation of China (No.2013CB834602). The DFT calculations were performed in the Supercomputing Center of the University of Science and Technology of China.

[1] C. H. Zhou and Y. Wang, Curr. Med. Chem. **19**, 239 (2012).
[2] M. T. Fera, E. La Camera, and A. De Sarro, Expert Rev. Anti-Infect. Ther. **7**, 981 (2009).
[3] B. Japelj, S. Rečnik, P. čebašek, B. Stanovnik, and J. Svete, J. Heterocycl. Chem. **42**, 1167 (2005).
[4] A. P. G. Nikalje, M. S. Ghodke, F. A. K. Khan, and J. N. Sangshetti, Chin. Chem. Lett. **26**, 108 (2015).
[5] S. M. Rabea, N. A. El-Koussi, H. Y. Hassan, and T. Aboul-Fadl, Arch. Pharm. **339**, 32 (2006).
[6] V. Pande and M. J. Ramos, Bioorg. Med. Chem. Lett. **15**, 5129 (2005).
[7] M. Lagrenee, B. Mernari, M. Bouanis, M. Traisnel, and F. Bentiss, Corros. Sci. **44**, 573 (2002).
[8] W. H. Li, Q. He, S. T. Zhang, C. L. Pei, and B. R. Hou, J. Appl. Electrochem. **38**, 289 (2008).
[9] W. H. Li, Q. He, C. L. Pei, and B. R. Hou, Electrochimi. Acta **52**, 6386 (2007).
[10] B. Zhang, D. P. Zhou, X. G. Lv, Y. Xu, and Y. C. Cui, Desalination **327**, 32 (2013).
[11] P. Wu, A. K. Feldman, A. K. Nugent, C. J. Hawker, A. Scheel, B. Voit, J. Pyun, J. M. J. Frchet, K. B. Sharpless, and V. V. Fokin, Angew. Chem. Int. Ed. **43**, 3928 (2004).
[12] S. G. Agalave, S. R. Maujan, and V. S. Pore, Chem. Asian J. **6**, 2696 (2011).
[13] L. Ackermann, H. K. Potukuchi, D. Landsberg, and R. Vicente, Org. Lett. **10**, 3081 (2008).
[14] B. Pergolese, M. Muniz-Miranda, and A. Bigotto, Vib. Spectrosc. **48**, 202 (2008).
[15] B. Pergolese, M. Muniz-Miranda, and A. Bigotto, J. Phys. Chem. B **109**, 9665 (2005).
[16] B. Pergolese, M. Muniz-Miranda, and A. Bigotto, J. Phys. Chem. B **108**, 5698 (2004).
[17] B. Pergolese and A. Bigotto, J. Mol. Struct. **651-653**, 349 (2003).
[18] M. Muniz-Miranda, F. Muniz-Miranda, and S. Caporali, Beilstein J. Nanotechnol. **5**, 2489 (2014).
[19] J. Sarkar, J. Chowdhury, and G. B. Talapatra, J. Phys. Chem. C **111**, 10049 (2007).
[20] R. Zhang, H. F. Yang, Y. P. Sun, W. Song, X. Zhu, N. Wang, Y. Wang, Y. C. Pan, and Z. R. Zhang, J. Phys. Chem. C **113**, 9748 (2009).
[21] Y. P. Sun, W. Song, X. Zhu, R. Zhang, Q. Y. Pang, Z. R. Zhang, and H. F. Yang, J. Raman Spectrosc. **40**, 1306 (2009).
[22] Y. C. Pan, Y. Wen, R. Zhang, Y. Y. Wang, Z. R. Zhang, and H. F. Yang, Appl. Surf. Sci. **258**, 3956 (2012).
[23] P. Piotrowski, B. Wrzosek, A. Królikowska, and J. Bukowska, Analyst **139**, 1101 (2014).
[24] B. Wrzosek, J. Cukras, and J. Bukowska, J. Raman Spectrosc. **43**, 1010 (2012).
[25] B. Wrzosek, J. Cukras, M. A. Dobrowolski, and J. Bukowska, J. Phys. Chem. C **121**, 9282 (2017).
[26] S. Meng, Y. Y. Zhao, J. D. Xue, and X. M. Zheng, Spectrochim. Acta A: Mol. Biomol. Spectrosc. **190**, 478 (2018).
[27] Y. Q. Yu, W. Fan, Y. X. Wang, X. G. Zhou, J. Sun, and S. L. Liu, J. Phys. Chem. B **121**, 8179 (2017).
[28] Y. X. Wang, K. Lin, L. Chen, X. G. Zhou, and S. L. Liu, Chin. J. Chem. Phys. **30**, 365 (2017).
[29] A. D. Naik, M. M. Dîrtu, A. Léonard, B. Tinant, J. Marchand-Brynaert, B. L. Su, and Y. Garcia, Cryst. Growth Des. **10**, 1798 (2010).
[30] M. H. Ryu, J. W. Choi, H. J. Kim, N. Park, and B. K. Cho, Angew. Chem. Int. Ed. **50**, 5737 (2011).
[31] Y. Li, W. Q. Zou, M. F. Wu, J. D. Lin, F. K. Zheng, Z. F. Liu, S. H. Wang, G. C. Guo, and J. S. Huang, CrystEngComm **13**, 3868 (2011).

DOI:10.1063/1674-0068/cjcp1903060 

[32] V. Safarifard and A. Morsali, CrystEngComm **14**, 5130 (2012).
[33] S. W. Zhang, W. Shi, and P. Cheng, Coord. Chem. Rev. **352**, 108 (2017).
[34] Y. Yang, F. L. Jiang, C. P. Liu, L. Chen, Y. L. Gai, J. D. Pang, K. Z. Su, X. Y. Wan, and M. C. Hong, Cryst. Growth Des. **16**, 2266 (2016).
[35] B. Ding, E. C. Yang, J. H. Guo, X. J. Zhao, and X. G. Wang, Inorg. Chem. Commun. **11**, 1481 (2008).
[36] Ş. Yurdakul and S. Tanrıbuyurdu, Struct. Chem. **23**, 433 (2012).
[37] H. S. Yu, X. He, S. H. L. Li, and D. G. Truhlar, Chem. Sci. **7**, 5032 (2016).
[38] M. A. Palafox, J. Phys. Chem. A **103**, 11366 (1999).
[39] M. J. Frisch,G. W. Trucks, H. B. Schlegel, G. E. Scuseria, M. A. Robb, J. R. Cheeseman, G. Scalmani, V. Barone, G. A. Petersson, H. Nakatsuji, X. Li, M. Caricato, A. V. Marenich, J. Bloino, B. G. Janesko, R. Gomperts, B. Mennucci, H. P. Hratchian, J. V. Ortiz, A. F. Izmaylov, J. L. Sonnenberg, D. Williams-Young, F. Ding, F. Lipparini, F. Egidi, J. Goings, B. Peng, A. Petrone, T. Henderson, D. Ranasinghe, V. G. Zakrzewski, J. Gao, N. Rega, G. Zheng, W. Liang, M. Hada, M. Ehara, K. Toyota, R. Fukuda, J. Hasegawa, M. Ishida, T. Nakajima, Y. Honda, O. Kitao, H. Nakai, T. Vreven, K. Throssell, J. A. Montgomery, Jr., J. E. Peralta, F. Ogliaro, M. J. Bearpark, J. J. Heyd, E. N. Brothers, K. N. Kudin, V. N. Staroverov, T. A. Keith, R. Kobayashi, J. Normand, K. Raghavachari, A. P. Rendell, J. C. Burant, S. S. Iyengar, J. Tomasi, M. Cossi, J. M. Millam, M. Klene, C. Adamo, R. Cammi, J. W. Ochterski, R. L. Martin, K. Morokuma, Ö. Farkas, J. B. Foresman, and D. J. Fox, *Gaussian 16, Revision A.03*, Wallingford CT: Gaussian, Inc.,(2016).
[40] P. L. Polavarapu, J. Phys. Chem. **94**, 8106 (1990).
[41] G. Keresztury, S. Holly, G. Beseznyei, J. Varga, A. Y. Wang, and J. R. Durig, Spectrochim. Acta A: Mol. Spectrosc. **49**, 2007 (1993).
[42] M. H. Jamróz, *Vibrational Energy Distribution Analysis: VEDA 4 Program*, Warsaw, (2004).
[43] M. H. Jamróz, Spectrochim. Acta A: Mol. Biomol. Spectrosc. **114**, 220 (2013).
[44] Z. L. Zhang, W. L. Wang, S. L. Liu, and D. M. Chen, Chin. J. Chem. Phys. **30**, 7 (2017).

DOI:10.1063/1674-0068/cjcp1903060 